Article

Journal of Vibration and Control
1–17

DOI: 10.1177/1077546314533584
jvc.sagepub.com

Vibration-based delamination detection in composite beams through frequency changes

Zhifang Zhang[1,2], Krishna Shankar[2], Evgeny V Morozov[2] and Murat Tahtali[2]

Abstract

Delamination is a common damage in fibre reinforced composite laminates, usually hidden from external view, that can substantially reduce the structural stiffness which changes the dynamic response of the structures such as natural frequencies. Natural frequencies are the most reliable parameters for detecting damage while they do not directly provide information regarding its location and severity. To determine the location and severity of damage, it is necessary to solve the inverse problem using frequency shifts in multiple modes. In this paper, the graphical approach, which was previously employed for estimating two variables of crack (location and size) in isotropic beams, is extended in the current work to estimate the three variables of delamination (interface, span-wise location and size) in anisotropic composite beams from measured frequency shifts. Compared to the use of optimisation or neural network for detection, graphical technique is computationally inexpensive and quick since it solves the inverse problem without iterations or network training. The present approach has been validated using numerical simulation as well as experimental data from modal testing conducted on quasi-isotropic simply supported and cantilever beams. Results show that the proposed graphical technique can be used to assess the location and severity of delamination in composite beams with a high degree of accuracy.

Keywords

Delamination detection, natural frequency, composite laminate, structural health monitoring, vibration

1. Introduction

Fibre-Reinforced Polymer (FRP) composites are widely used in aeronautical, marine and automotive industries, because of their excellent mechanical properties, low density, better fatigue and corrosion resistance and manufacturability. However, it is widely acknowledged that FRP laminates are susceptible to impact damage and prone to developing damage in the form of delaminations due to low inter-laminar strength (Zou and Tong, 2000). Since they occur inside the laminate, delaminations are insidious, causing significant reductions in the flexural stiffness and compressive buckling strength of the structure. Hence industries spend considerable time and effort in inspecting for delaminations using techniques such as ultrasonic scanning, X-ray and thermographs. The current trend, especially in the aerospace industry, is to turn to Structural Health Monitoring (SHM) systems (Sohn et al., 2003; Montalvao et al., 2006), which can monitor the integrity of the structure online and *in situ*, thus increasing safety as well as reducing costs due to aircraft down time. The SHM techniques currently available for detecting delaminations in composites include guided-wave based techniques, acoustic emission, optical fibre gratings, impedance-based method,

[1]Guangzhou University - Tamkang University Joint Research Center for Engineering Structure Disaster Prevention and Control, Guangzhou, China
[2]School of Engineering and Information Technology, University of New South Wales at Canberra, Australia

Received: 17 December 2013; accepted: 28 March 2014

Corresponding author:
Zhifang Zhang, Guangzhou University - Tamkang University Joint Research Center for Engineering Structure Disaster Prevention and Control, Guangzhou, China.
Email: zzfbusi@gmail.com

comparative vacuum monitoring, and vibration monitoring (Doebling and Farrar, 1996; Yan et al., 2007; Fan and Qiao, 2010; Raghavan and Cesnik, 2007; Xiang and Liang, 2012; Xiang et al., 2013). While considerable research efforts have been expended in the development of all the above mentioned SHM technologies, vibration-based SHM is the main focus of the research reported here. The principle behind vibration based damage detection is that damage in a structure reduces its local stiffness which results in changes in dynamic parameters such as natural frequencies, mode shapes and damping ratios (Fritzen, 2005; Della and Shu, 2007). Therefore, by monitoring changes in these parameters damage can be detected and assessed. The monitoring of mode shapes requires measurements at multiple locations, therefore it is time consuming and prone to noise which may eliminate the effect of damage. Damping parameters are notoriously difficult to measure, and are sensitive to environmental conditions such as humidity and temperature. In comparison, natural frequencies can be measured with a single sensor, and can be monitored with greater accuracy, ease and reliability (Salawu, 1997; Kessler et al., 2002; Yang et al., 2013). Frequency based vibration monitoring systems facilitate global monitoring, can be retrofitted and removed easily, and provide reliable and accurate data. Further, especially in aircraft, they do not need an input source for excitation, since the vibration of structural components while in operation can be captured and frequency can be extracted for monitoring structural integrity. A reduction in stiffness will reduce the natural frequencies of the structure, so the incidence of damage can be detected simply by monitoring the natural frequencies for a significant and permanent shift downwards. This is one of the major advantages of frequency based vibration monitoring. However, an associated disadvantage is that while the presence of damage is globally detected, the drop in frequency provides no clue as to its location and only a qualitative indication of its severity, which is dependent on the location. The full assessment of the damage requires the solution of the inverse problem, i.e., determination of the location and severity of damage from measured changes in multiple modal frequencies. Previous researchers have mainly resorted to advanced system identification or artificial intelligence such as neural networks (Chakraborty, 2005; Okafor et al., 1996; Valoor and Chandrashekhara, 2000; Islam and Craig, 1994; Wei et al., 2005) and genetic algorithm (Su et al., 2005; Ihesiulor et al., 2012). However, when only two or three parameters are to be determined, such as location along the length of the beam, the depth at which it occurs and the size of the delamination, it can be easily determined using a graphical technique (Zhang et al., 2011). The advantage of the graphical technique is that it solves the inverse problem without iterations or network training, unlike typical optimisation methods and searching algorithms, and is therefore computationally inexpensive and easy to implement.

The graphical technique was first proposed by Adams and Cawley (1978), who showed that by plotting a crack size index versus crack location for the first three modes of a straight bar, the possible damage size and location of the crack can be estimated. Since then many researchers have employed a similar technique for solving the inverse problem, but mostly for estimating location and size of transverse or through thickness cracks in isotropic (metallic) beams (Patil and Maiti, 2005; Owolabi et al., 2003; Kim and Stubbs, 2003; Springer et al., 1988) which are two-variable problems. Delamination in composite laminates, however, is different from cracks in isotropic materials, not only due to the complexity added by the anisotropic nature of the material but also because there is one extra characteristic parameter to be determined, which is the interfacial location of the delamination. In this paper, for the first time, the graphical approach is extended to determine three variables, the x & z locations and the size of delaminations in laminated composite beams. The proposed technique is validated by numerical simulation data and then applied for assessment of delaminations in simply supported and cantilever Carbon Fibre Reinforced Polymer (CFRP) beam specimens with artificially induced delaminations.

2. Finite element modelling

The forward problem, that is determination of frequency shifts as functions of the damage parameters, can be solved either analytically or by finite element modelling. In this paper we built the FE model for laminated beams to determine the natural frequencies of CFRP beams with delaminations and generate the data for application of the proposed graphical technique for delamination assessment in the numerical validation. The finite element modelling for simulation of the delaminated beams and extraction of the natural frequencies was conducted using the modal analysis option in the commercial software ANSYS12.

Layered Solid185 was employed for modelling the delaminated beams, with one element for each layer across the thickness. The layer information is defined by using shell section. A mesh sensitivity study was conducted to determine the optimum number of elements to be employed for the delaminated beam model. The final model employed 200 elements along the length, six along the width and one element for each layer of the laminate. The delaminated beam was modelled as two volumes, separated along the interface

XML Template (2014) [16.5.2014–11:04am] [1–17]
//blmas3/cenpro/ApplicationFiles/Journals/SAGE/3B2/JVCJ/Vol00000/140100/APPFile/SG-JVCJ140100.3d (JVC) [PREPRINTER stage]

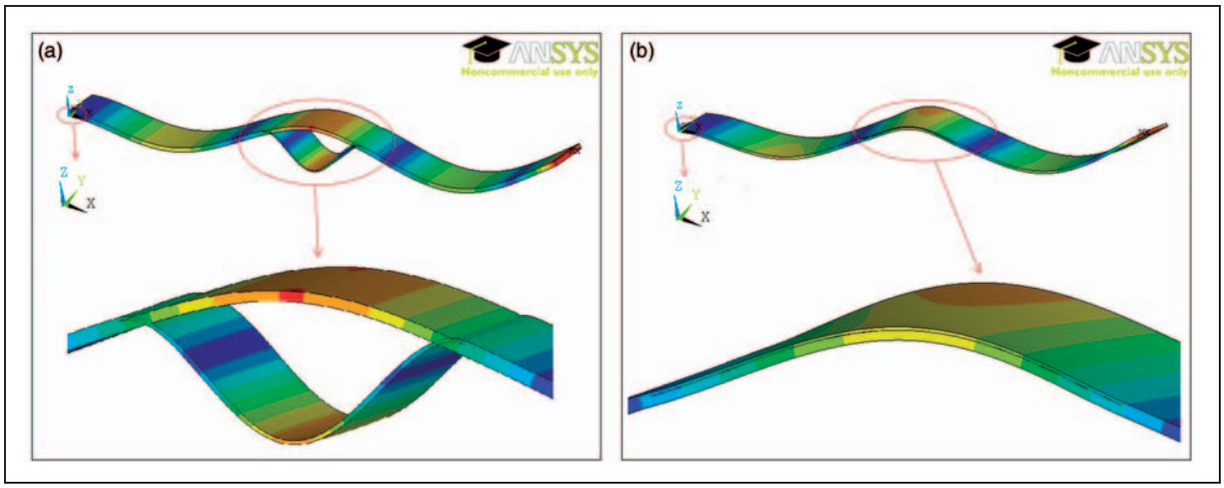

Figure 1. FE model of delaminated beam (a) without contact elements and (b) with contact elements between sub-laminates.

at which the delamination is located. The nodes locating along the interface of undelaminated segment were merged together while nodes in interface of delaminated area are left to be separate. If no contact is modelled between the nodes on the neighbouring surfaces of the upper and lower sub-laminates, the two sub-laminates can separate or inter-penetrate (Zhang et al., 2010), as in the 'free model' of Ramkumar et al. (1979) and Wang and Liu (1982), as shown in Figure 1(a). To obtain a more realistic representation of the behaviour of a real delamination, contact elements (TARGE170/CONTAC173) were introduced between the delaminated surfaces to prevent inter-penetration between the sub-laminates (see Figure 1(b)), as in the 'constrained model' of Mujumdar and Suryanarayan (1988) and Grouve et al. (2008). The contact is implemented with the 'Standard' contact behaviour in ANSYS12, which introduces normal pressures to prevent the surfaces from overlapping and sets the normal pressure to zero if separation occurs. In non-linear analysis such as transient analysis, this would allow the sub-laminates to separate. However, the frequencies of the delaminated beams in this study are determined using the modal analysis option in ANSYS, which is a linear Eigen value solution. Being linear, 'any nonlinear contact retains the initial status throughout the modal analysis and the stiffness contribution from the contact is based on the initial status and never changes' as per the ANSYS manual (2009). Hence no separation is seen in the modal analysis of the delaminated FE models even though 'Standard' contact allows separation. Finally, the torsion and in-plane bending modes were discarded and only the flexural modes retained to develop the database for the damage detection algorithm.

3. Descriptions of experiments

3.1. Fabrication of CFRP beams with artificial delaminations

The graphite-epoxy panels for the beam samples employed in the tests were fabricated with MTM57/PANEX35 unidirectional prepreg tapes using hand lay-up and vacuum assisted consolidation process and heater blankets at a cure temperature of 120 degrees Celsius as per the manufacturer's cure cycle. The panels manufactured were 8 ply symmetric balanced laminates with a quasi-isotropic lay-up of $[0/-45/45/90]_s$. The delaminations were simulated by embedding a pair of Teflon release films of the required size between the layers at the predetermined interfaces and locations. For a composite beam with length L, width W and thickness t, the parameters for the through-width delamination are: the axial location of the delamination x, the interface location z (transverse coordinate), and the delamination size a (axial length of the through width delamination), as shown in Figure 2. After cure, each panel was cut with a diamond saw into coupons of the required width. A thin metal sheet was inserted between the release films to ensure complete separation between the sub-laminates. An optical microscope was then employed to examine the delamination edges on both sides and measure their actual sizes. A total of seven beam samples with delaminations and one control sample without delamination were cut from the manufactured quasi-isotropic CFRP panels. The manufactured beams had a length of 260 mm and a nominal width of 19.25 mm. The widths and thicknesses of the individual beams, along with the delamination sizes and locations are listed in Table 1. In this paper, the interfaces are numbered

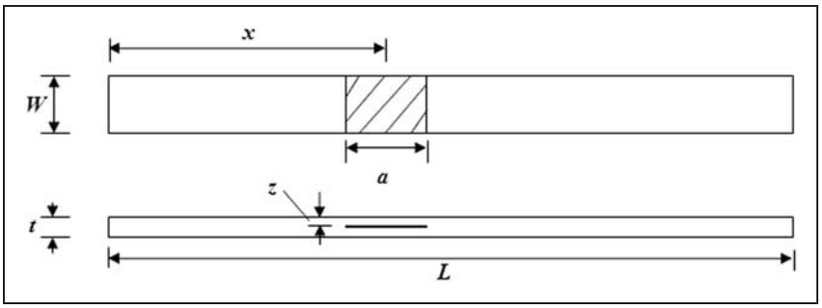

Figure 2. Dimensions and delamination parameters in composite beam.

Table 1. Specimen dimensions and delamination characteristics.

Beam ID	Width (mm)	Thickness (mm)	Delamination interface	Delamination size (mm)	Cantilever x-location[a] (mm)	SS x-location[b] (mm)
8# (intact)	19.18	2.27				
1#	19.25	2.46	4	28	44.9	52.1
2#	19.09	2.66	3	31	45.3	52.5
3#	19.29	2.76	2	33	43.3	50.5
4#	19.36	2.76	2	60.2	105.1	112.3
5#	19.1	2.79	2	44.3	103.2	110.4
6#	19.14	2.8	2	30.6	104.3	111.5
7#	18.98	2.69	1	34.5	43	50.2

[a]Distance from fixed end of cantilever, [b]distance from left end of S.S. beam.

1 to 4, from the outermost interface to the mid-plane. The thicknesses listed against the beams in Table 1 are average values of measurements taken at over 20 locations along their length. It may be noted that beams 3 to 6 have fairly uniform thickness (about 2.8 mm), while the beams above and below have lower thickness. This is because the composite panel, which was cured under vacuum compression, was thicker in the middle and tapered towards the edges. In particular, the beam without delaminations (intact beam) has a much lower average thickness, 2.27 mm, only about 82% of the average thickness of the delaminated beams.

3.2. Experimental set-up

Experimental modal analysis was conducted on the beam samples using Polytec scanning vibrometer (PSV) first with simply supported boundary conditions. Then the same samples were clamped at one end and tested as cantilever beams. Figure 3(a)–(c) show the experimental set-up employed for modal testing of the simply supported beams. The laser scan head on its tripod is shown in Figure 3(a); Figure 3(b) shows the specially designed and constructed steel blocks, with slots for the 30 mm diameter rollers which provided simple support boundary conditions at either end of the beam. The beams were mounted horizontally on steel blocks near the floor and the scan head of the laser scanning vibrometer (seen in Figure 3(a)) mounted on a tripod pointing downwards at it. Figure 3(c) shows the laser beam shining down on the horizontal beam and the loudspeaker below which was used to excite the beam. For cantilever boundary condition, the beams were clamped upright in a vice using torque wrench to guarantee 30Nm for each fixture and the laser beam from the scan head travelled horizontally to scan the length of the cantilever vertically. The span of the simply supported beams between the roller supports was 242 mm and the length of the cantilever beams, excluding the clamped region, was 240 mm.

3.3. Experimental modal analysis

The experimental modal analysis was conducted using a PSV-400 non-contact scanning laser Doppler vibrometer (Figure 3(a)) and the data was processed using the software PSV8.7 to extract the natural frequencies. The measurement area of the simply supported beam (152 mm × 20 mm) was set up to a grid of 3 × 33 to provide 99 measurement points (45 mm at either end

XML Template (2014) [16.5.2014–11:04am] [1–17]
//blmas3/cenpro/ApplicationFiles/Journals/SAGE/3B2/JVCJ/Vol00000/140100/APPFile/SG-JVCJ140100.3d (JVC) [PREPRINTER stage]

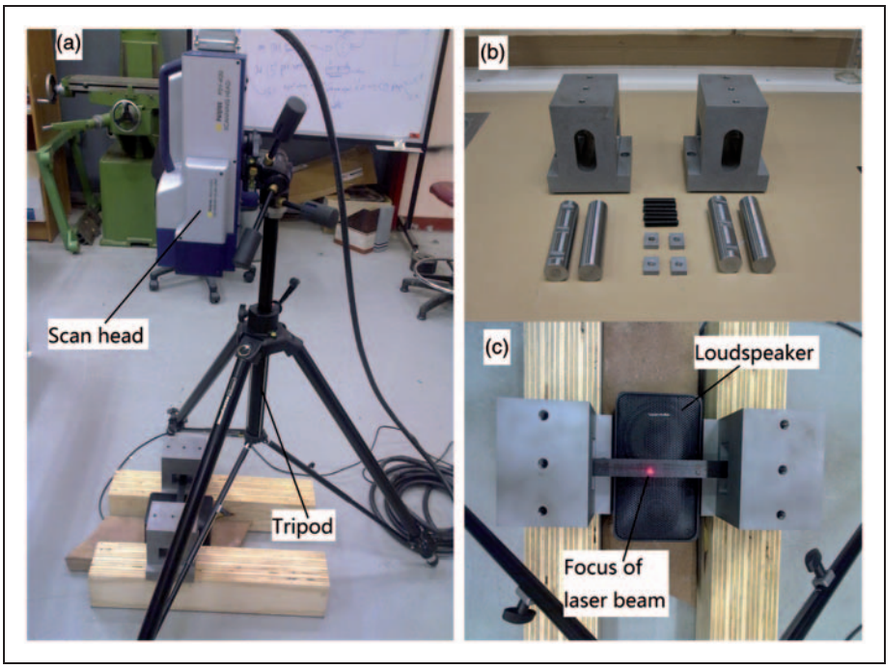

Figure 3. Experimental set-up for simply supported beams (a) laser scan head (b) simple support fixture and (c) loudspeaker used for excitation and scanning laser beam.

Table 2. Measured frequencies of simply supported beams (Hz).

Beam ID	Mode 1	Mode 2	Mode 3	Mode 4	Mode 5	Mode 6	Mode 7
8# (intact)	135	465	1068	1837	2819	3940	5313
1#	141	508	1266	1712	2696	4017	5149
2#	148	542	1338	1675	2931	4332	5582
3#	152	548	1352	1915	2944	4419	6034
4#	152	465	1247	1675	2750	3659	5009
5#	162	523	1336	1845	3049	4344	5348
6#	156	540	1394	1977	3194	4206	5748
7#	145	526	1284	1999	3064	4348	6111

of the beam was hidden from the laser head by the simply support mounting blocks). The response at each measurement point was averaged 15 times to improve the signal-to-noise ratio. A frequency range of 0 to 6400 Hz was selected since the eighth modal frequency obtained from FE model for the undamaged beam had a value of about 6000 Hz. The Fast Fourier Transform (FFT) lines were set to be 12800 providing a resolution of 0.5 Hz. The non-contact excitation was provided with sound from a loudspeaker behind the specimen with sweep signal from 1 Hz to 10000 Hz in 0.5 s (Montalvao et al., 2009). The frequencies were estimated by the software within the bandwidths spanning the peaks in the frequency spectrum. The corresponding mode shapes were examined to check that only flexural modes in the right sequences have been selected. Tables 2 and 3 list the first seven modal frequencies obtained from the tests on the simply supported beams and the cantilever beams, respectively. It may be noted that the measured frequencies of the intact beams are mostly lower than those of the delaminated beams, contrary to expectations that damage reduces beam stiffness and hence natural frequencies. The lower frequencies of the intact beam in this case is due to its thickness being about 18% lower than those of the delaminated beams due to taper in the composite panels fabricated, as explained in section 3.1. Hence beams #1 to #7 have higher overall bending stiffness and, if they did not have delaminations, would have higher natural frequencies than the intact beam.

The reductions in natural frequencies through reductions in stiffness by the delaminations are lower in magnitude than the increments due to the higher thicknesses of beams #1 to #7. It is also to be mentioned that there is a small thickening effect locally due to the insertion of the Teflon sheets to simulate delaminations, but this is expected to have only a minor contribution since Teflon has a small stiffness. Comparing the natural frequencies of beams with delaminations of similar size and similar axial locations (beams 1, 2, 3 and 7) in Tables 2 and 3, it can be seen that, in general, as the location of delaminations moves from the outermost interface (interface 1) to the innermost (interface 4), the measured frequencies of the higher modes (modes 4–7) decrease, as expected and reported in the literature. This trend, however, is not seen for the lower modes. The discrepancy from expected trend in the lower modes may be attributed to the fact that there are greater uncertainties in measurements of lower frequencies in tests than higher frequencies, as reported in the literature, and variations in boundary conditions and beam dimensions in general have a greater effect on the lower modes. To determine the frequency shifts caused by the delaminations in the experimental beams, for experimental validation of the proposed damage assessment technique, the undamaged frequencies are estimated by FE simulation using the actual dimensions of the individual test beams, from which the measured experimental frequencies are subtracted for each mode.

3.4. Model updating

To implement any inverse algorithm using a data base of frequency shifts computed using numerical simulation, it is necessary to first ensure that the finite element model used in the simulation matches the real beams or test samples as closely as possible. Model updating is the means used for this by most researchers in SHM (Mottershead and Friswell, 1993). The model updating was conducted using the measured natural frequencies of the undamaged S.S. and cantilever beams using two parameters as variables: the fibre volume fraction of the CFRP laminate and the effective length of the cantilever beam. These two parameters were selected for model updating because of the uncertainty in the actual fibre volume fraction of the laminates fabricated with the hand layup technique and cured using the heater blankets and the uncertainty in the effective length of cantilever beams due to the difficulty of achieving perfect clamping at the built in edge. The fibre volume fraction in the FE model was updated with assistance of a single-objective optimisation to provide the minimum value for the root mean square (RMS) errors of the discrepancies between the predicted and measured frequencies of the undamaged S.S. beams, using material properties for the individual CFRP lamina from manufacturers specifications and the rule of mixtures (Altenbach et al., 2004) whose equations are shown below

$$E_{11} = E_f V_f + E_m(1 - V_f) \tag{1}$$

$$E_{22} = \frac{E_f E_m}{E_m V_f + E_f(1 - V_f)} \tag{2}$$

$$G_{12} = \frac{G_f G_m}{V_f G_m + (1 - V_f) G_f} \tag{3}$$

$$\upsilon_{12} = \upsilon_f V_f + \upsilon_m(1 - V_f) \tag{4}$$

where E_{11} and E_{22} are respectively the module in the longitudinal (zero degree) and transverse (ninety degree) directions, G_{12} and ν_{12} are in-plane shear modulus and the Poisson's ratio. E_f, E_m, G_f, G_m, and ν_f, ν_m, are the Young's Modulus, Shear Modulus and Poisson's ratios of the fibre and matrix respectively. The properties of the Panex35 carbon fibre and the MTM57 epoxy matrix were obtained from the manufacturer's data sheet (2004) as: $E_f = 229.8$ GPa, $E_m = 4.98$ GPa, $G_f = 22$ GPa, $G_m = 1.85$ GPa, $\nu_f = 0.3$

Table 3. Measured frequencies of cantilever beams (Hz).

Beam ID	Mode1	Mode 2	Mode 3	Mode 4	Mode 5	Mode 6	Mode 7
8# (intact)	40	248	698	1362	2244	3358	4656
1#	46	260	724	1482	2434	3054	4290
2#	50	286	792	1610	2636	3386	4628
3#	50	296	812	1632	2656	3544	4656
4#	48	276	704	1434	2402	3226	4524
5#	52	318	788	1530	2506	3178	4656
6#	50	310	826	1586	2568	3454	5228
7#	44	290	804	1564	2665	3730	5020

and $\nu_m = 0.345$. The only unknown in equations 1 to 4 is the fibre volume fraction, V_f, which had some uncertainty due to the hand layup process employed for manufacturing the samples. The fibre volume fraction, V_f, was determined by updating the FE model of the S.S. beam as described above and was obtained as 0.389. The material properties of the CFRP composite lamina were then determined with equations (1)–(4) as $E_{11} = 92.5\,\text{GPa}$, $E_{22} = 8.04\,\text{GPa}$, $G_{12} = 2.88\,\text{GPa}$, $\nu_{12} = 0.33$ and density $\rho = 1429.0\,\text{Kgm}^{-3}$.

These material properties were also employed for the cantilever beam, and its effective length was determined by updating the FE model of the cantilever beam by comparison with the measured frequencies. This length was found to be 244 mm, 4 mm longer than the overhang length of the beam in the experimental set-up.

4. Comparison of FE and experimental frequencies

4.1. Undamaged beams

The measured frequencies of the undamaged cantilever and simply supported beams are compared with those predicted by the FE model in Figure 4(a) and (b), respectively. As can be seen, for the undamaged beams, the numerical predictions match the measured frequencies well, with discrepancies generally less than 3%. This is to be expected as the material properties used in the FE models were estimated by matching the predictions of the models with the measured frequencies of the undamaged beams.

4.2. Beams with delaminations

On comparing the frequencies of the delaminated beams measured in the experiments with those predicted numerically with FE, it is found that the two match better and more consistently under the cantilever condition than in the simply supported condition. This may be because the boundary conditions implemented in the experiments are closer to the ideal conditions modelled in FE for the cantilever set up than the simply supported set-up. For illustration, the discrepancy between measured and numerical modal frequencies of delaminated beam #3 is shown in Figure 5(a) and (b) for the cantilever and simply supported beams, respectively. For cantilever beams, the discrepancy is within 3% for most modes for all seven specimens. However, for simply supported beams, modes 1 and 3 have large discrepancies between measurements and FE results which can go up to over 14%. For other modes, the matches are generally good and within 4%. The discrepancy between the measured frequencies and those estimated by the FE model can be attributed to the following reasons: (a) uncertainties and errors in frequency measurements, (b) differences between the actual material properties of the beams tested and those employed in the FE model, (c) the assumption of uniform thickness employed in the FE simulations, instead of the taper in the actual beams, which were thick in the middle and thinner at the ends, (d) the inability to reproduce in the experiments the ideal boundary conditions of simple support and full clamping modelled in the numerical simulation, and (e) the constrained FE model employed in this study does not consider the nonlinear opening behaviour of delamination during vibration which may exist in real tests.

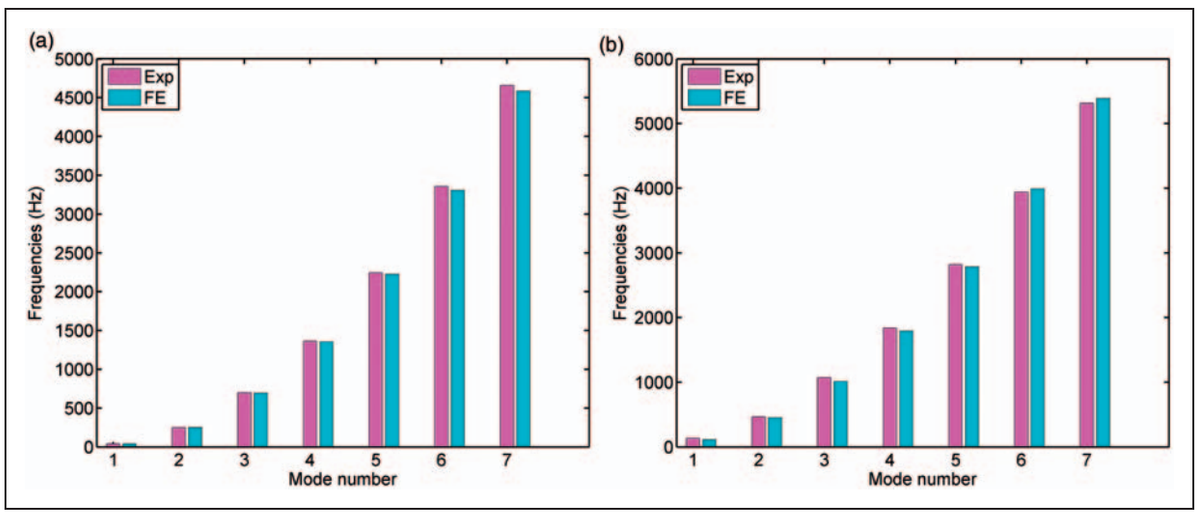

Figure 4. Comparison of frequencies from experiment and FE for undamaged beams (a) cantilever and (b) simply supported.

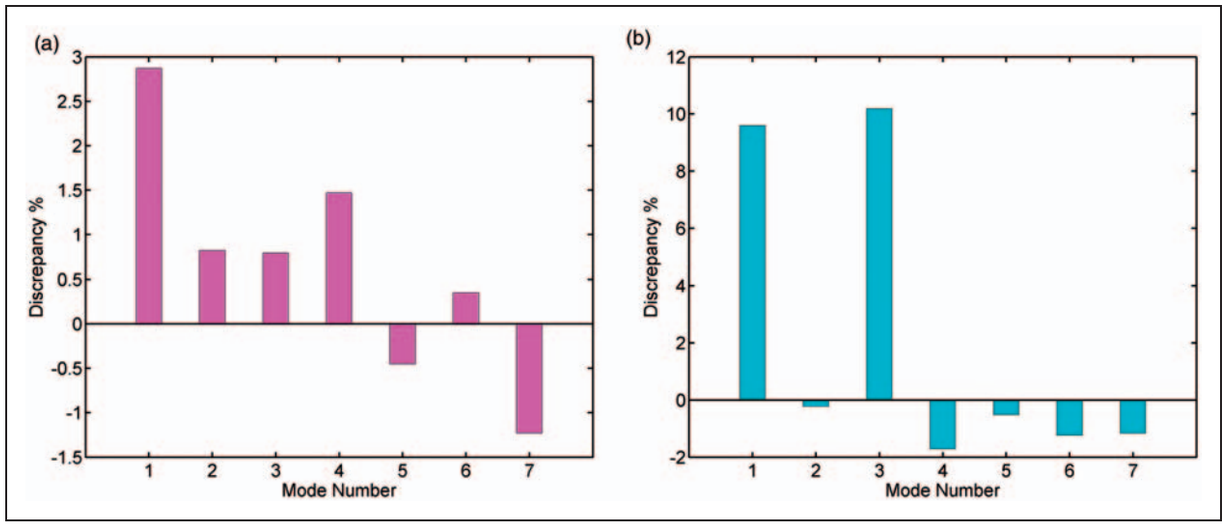

Figure 5. Comparison of frequencies from experiment and FE for delaminated beam #3 (a) cantilever and (b) simply supported.

5. Graphical technique for delamination assessment

5.1. Database and 3D plots of frequency shifts against delamination parameters

Assessment of delaminations from measured frequency changes requires a database of frequency shifts versus delaminations parameters to be generated first. The percentage frequency shift in each mode 'i' due to the delamination can be expressed as a function of the delamination size 'a', the axial location 'x' and the interface location 'z' as follows

$$\Delta\omega_i = \frac{\omega_{ui} - \omega_{di}}{\omega_{ui}} * 100 = f_i(a, x, z) \tag{5}$$

where ω_{ui} and ω_{di} are respectively frequencies of the undelaminated and the delaminated beams in the ith mode. For numerical validation, ω_{di} is obtained from FE model while for experimental validation, it is from measurements. In both numerical and experimental validations, the undamaged beam frequencies ω_{ui}, however, are obtained from FE model only as explained in section 3.3.

The database of frequency shifts against a range of normalised delamination size (a/L) normalised x-location (x/L) and interface location for both cantilever and simply supported composite beams with a lay-up of $[0/-45/45/90]_s$ were generated using FE modelling. For illustration, the 3D surface plots of the frequency shifts in modes 1 to 3 against normalised x-location and size for a delamination (at mid-plane) in the simply supported beam are shown in Figure 6.

From the 3D plots in Figure 6, it can be seen that the frequency shift in each mode monotonically increases with increasing delamination size; which is attributable to the reduction in overall stiffness of the beam with increasing damage size. However, the variation of frequency shift with the axial location of the delamination has many peaks and troughs, which seem to correspond with the mode shape, or more accurately, the variation of curvature along the length of the beam in each mode. Figure 7(a) and (b) show the variation of frequency shift versus x-location in mode 3 with fixed size of $a/L = 4\%$ and 40% respectively of delamination at interfaces 1 to 4 for simply supported end conditions. As the delamination goes deeper into the beam, the frequency shift causes increases, since, in general, the stiffness loss increases with increasing depth of delamination (Mujumdar and Suryanarayan, 1988). Figure 8(a)–(c), respectively show the variations of the deflection w (mode shape), magnitude of second derivative d^2w/dx^2 (curvature), and magnitude of third derivative d^3w/dx^3 (which is proportional to shear force) along the length of the beam in mode 3. Note that the values are normalised with respect to the maximum value in the figures.

Comparing the plots in Figures 7 and 8, we can see that the peaks and troughs in the frequency shifts of caused by a small delamination (Figure 7(a)) match the peaks and troughs of the absolute value of curvature (Figure 8(b)), whereas, when the delamination is large (Figure 7(b)), the variation in frequency shift along the length of the beam matches that of the third derivative, which is proportional to the shear variation in the beam (Figure 8(c)). The latter matches the conclusion by Tracy and Pardoen (1988) based on their study of a

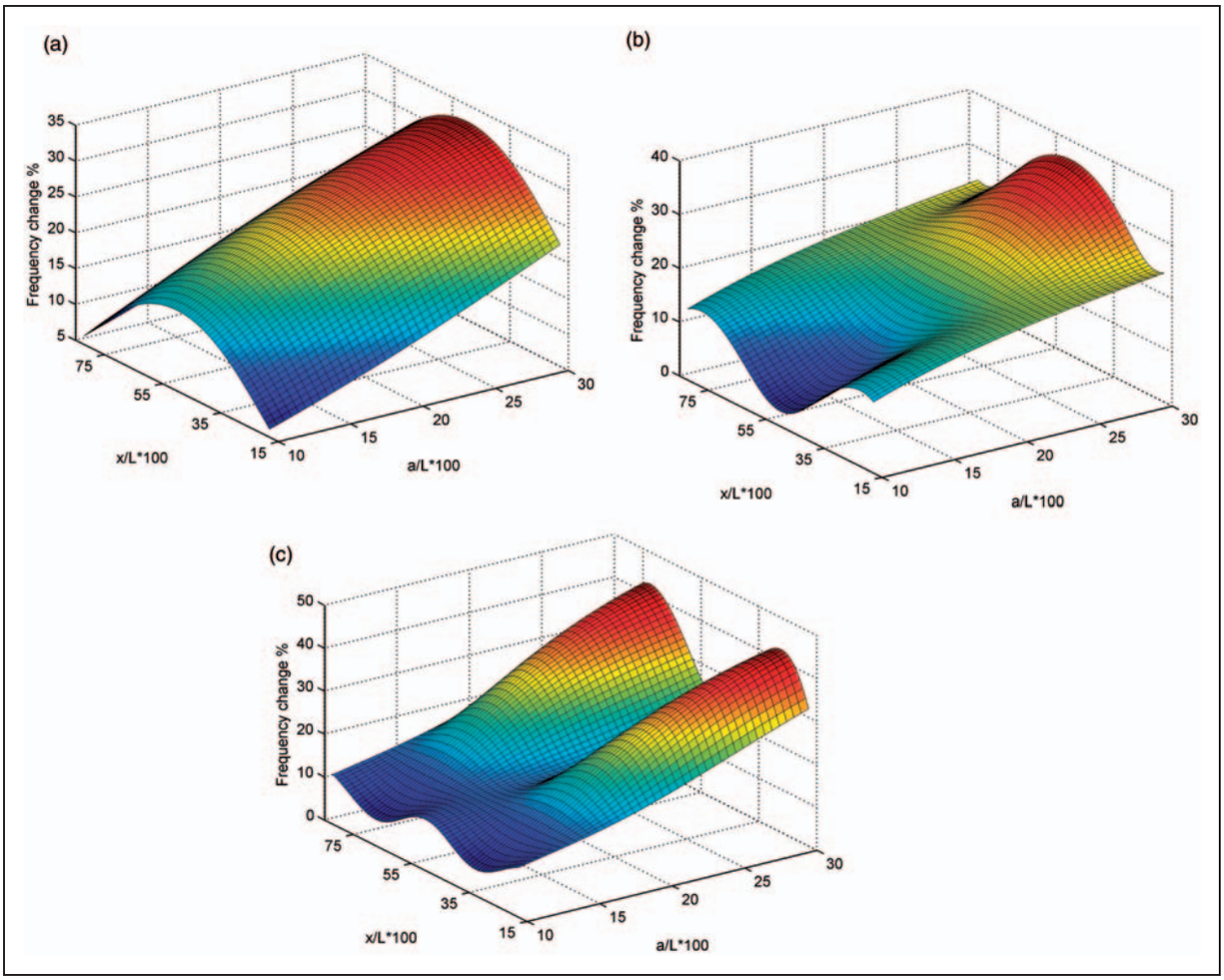

Figure 6. 3D plot of frequency shift against x-location and size of delamination in simply supported beam (a) mode 1, (b) mode 2 and (c) mode 3.

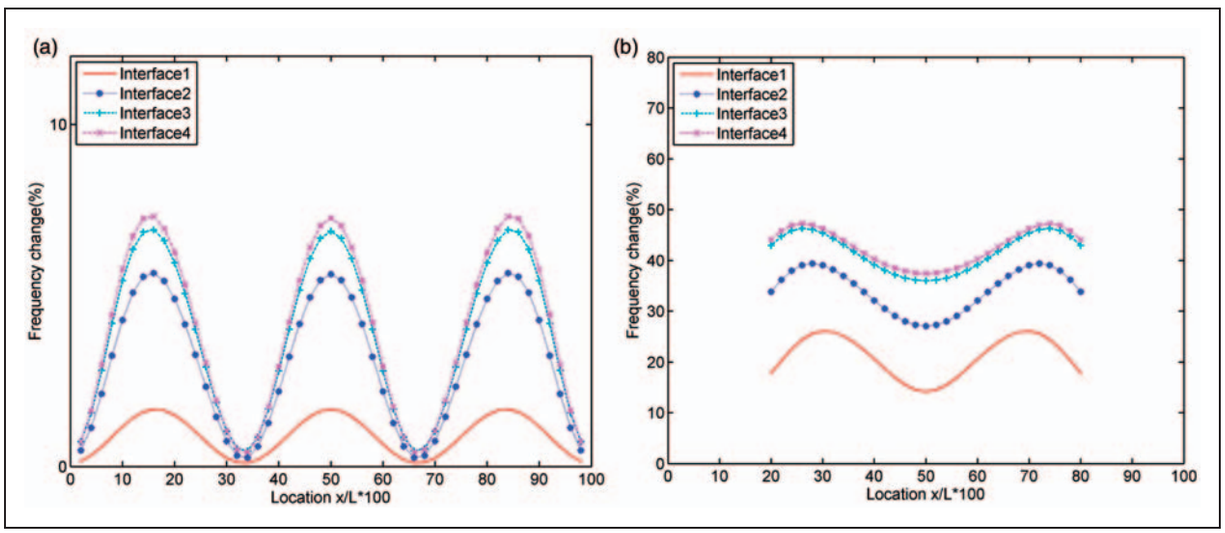

Figure 7. Variation of frequency shift with x-location in mode 3 for (a) small delamination ($a/L = 4\%$) and (b) large delamination ($a/L = 40\%$).

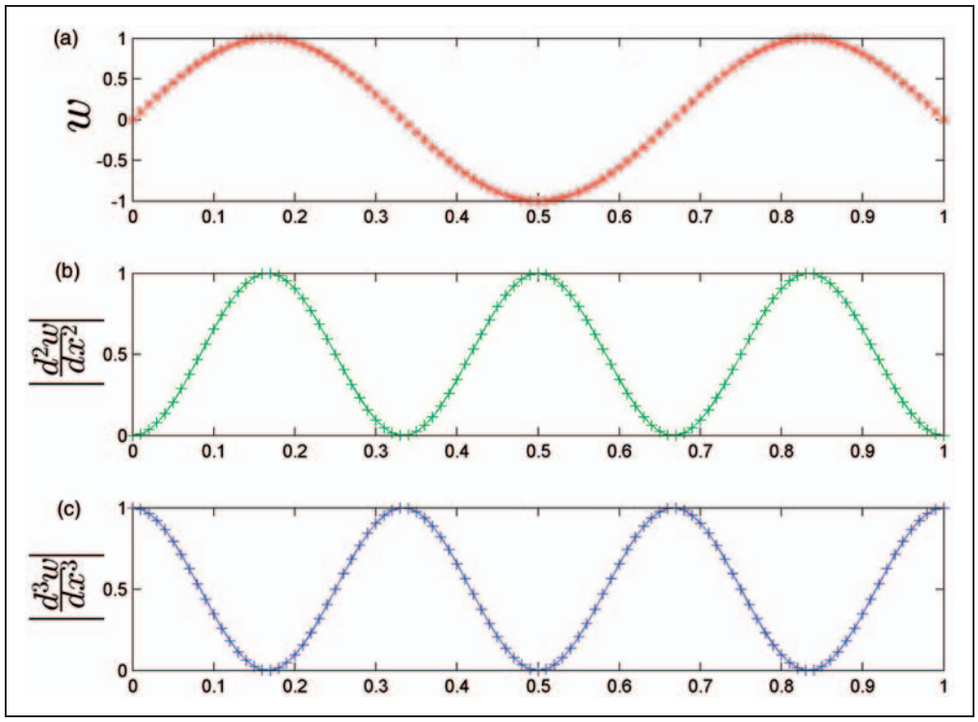

Figure 8. (a) Mode shape, (b) curvature and (c) shear force of simply supported beam in mode 3.

delamination with fixed size of 25%, that is, the delamination effects are much stronger in the regions with high shear than those with high curvature. However, present study of both small and large delaminations provides a more comprehensive insight to the delamination effects-depending on the damage size, the effect of delamination can be stronger in the regions of either high curvature or high shear force.

5.2. Damage assessment methodology

The inverse problem consists of determining the delamination parameters from measured shifts in frequencies. If frequency shifts in N modes ($N>=3$) are known, then equation (5) would give us a system of N equations ($i=1$ to N) which could be solved simultaneously to determine the three unknowns a, x and z; however, relationships between frequency shifts and delamination parameters are not explicitly known and are highly non-linear. The inverse problem is usually solved using a search algorithm such as GA or NN which requires iteration or network training; however, with only three parameters to be determined, it is expedient to do it using a graphical approach, both in terms of effort and computational time, with no loss in accuracy.

For each interface, the frequency shifts in each mode can be plotted against the delamination location 'x' and size 'a' to provide a 3D surface, as shown in Figure 9 for the first three modes for a quasi-isotropic cantilever beam with delamination at mid-plane. The known frequency shifts in these modes would represent horizontal planes in x-a space and intersect the 3D surfaces along 2D curves (shown in red in Figure 9(a)–(c), available online).

If the intersection curves of the known frequency shifts with the surface plots are plotted on a 2D plot of 'x' vs. 'a', all the curves will pass through the same (x, a) point under the assumption that a single delamination exists, providing the correct values of the x-location and size of the delamination, if the interface is chosen correctly, as indicated by a red dot in Figure 10(a). However, it can be observed that there is only one point at which all four curves intersect ($x=30.99$, $a=15.98$, indicated by the red dot); although there is another ($x=64.92$, $a=19.38$) at which three of the curves intersect. This highlights the need to use data from more modes than the number of unknown variables in order to obtain a singular set of solutions. In the current work frequency shifts from seven modes were employed in the graphical technique to ensure that a unique solution is attained. However, if the measured frequency shifts are employed to obtain intersection curves from surface plots of predicted frequency shifts for delamination at any other interface, the intersection plots of size vs. x-location for different modes will not all pass through the same point, as illustrated in Figure 10(b) for interface 2, since it is unlikely that any other combination of x, z and a will cause the

XML Template (2014) [16.5.2014–11:05am] [1–17]
//blmas3/cenpro/ApplicationFiles/Journals/SAGE/3B2/JVCJ/Vol00000/140100/APPFile/SG-JVCJ140100.3d (JVC) [PREPRINTER stage]

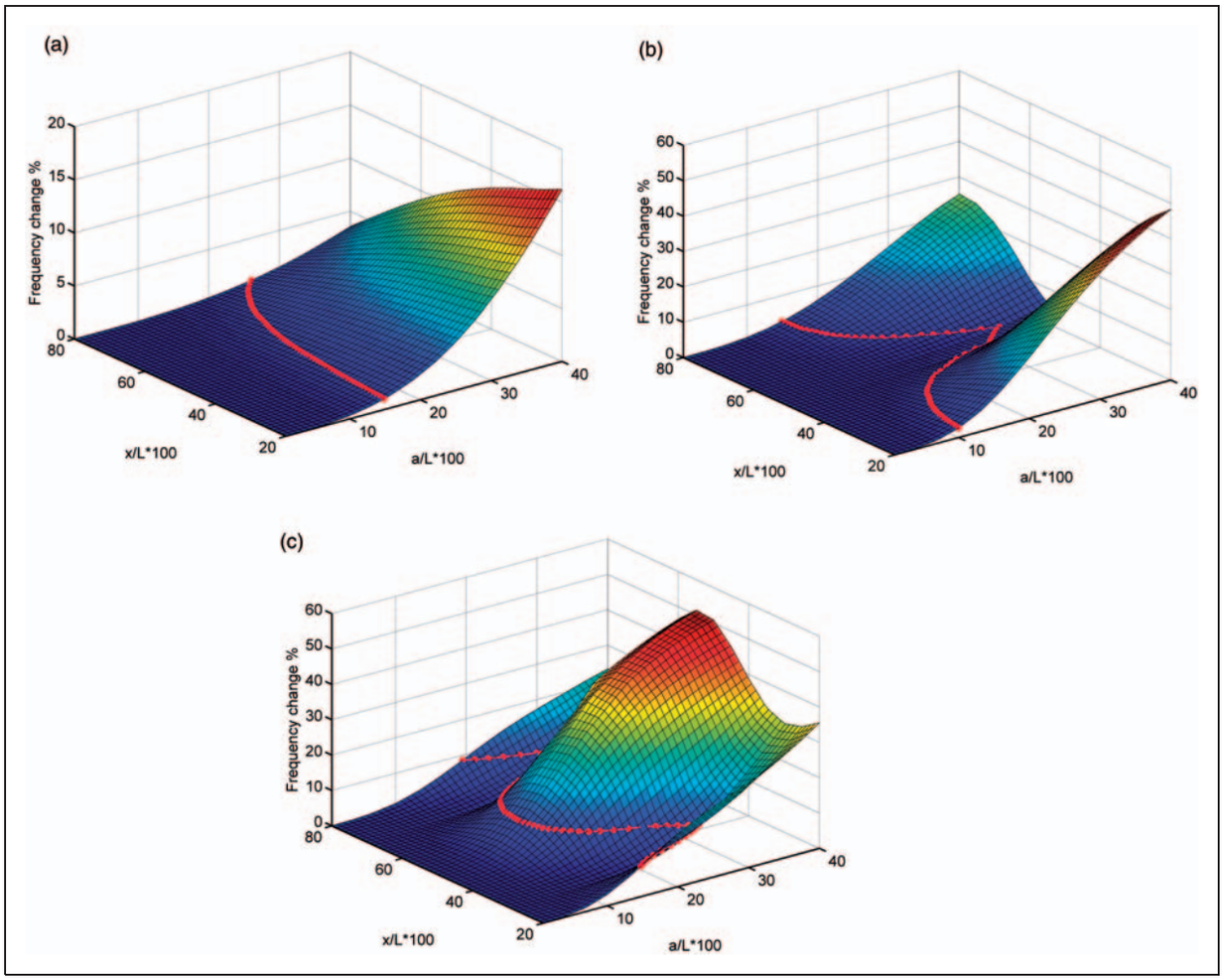

Figure 9. Intersections of known frequency shifts and surface plots of frequency shifts against delamination size and x-location at interface 4 for the first three modes.

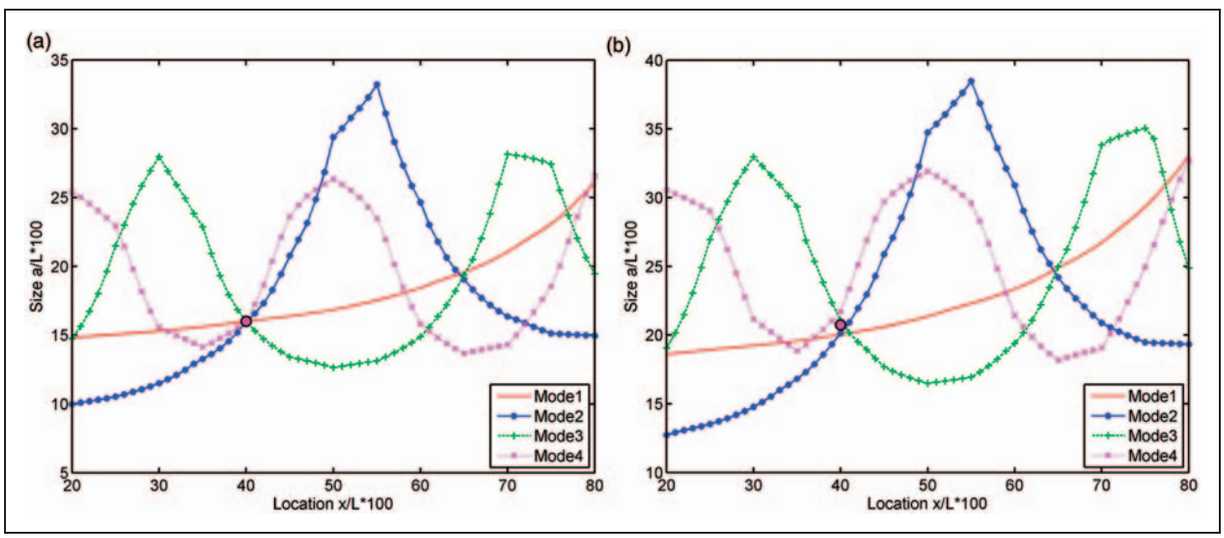

Figure 10. Size vs. x-location curves representing known frequency shifts in modes 1 to 4 (a) intersecting at a single point for the correct delamination interface (interface 4) and (b) intersecting at different points for a wrong interface (interface 2).

same shifts in frequencies as the measured ones, especially when the number of modes used for identification is much larger than three.

The size vs. x-location curves representing known frequency shifts for multiple modes will meet at a single point for the correct interface only in the ideal case. In practice, due to the approximations involved in developing the 3D surface plots (spline fits) from discrete data points, and errors in the measured frequency shifts, even for the correct interface, all the size vs. x-location curves will not meet at a single point, but will meet each other in the vicinity of the correct values of x and a. The standard deviation between the intersection curves for different modes will be a minimum (zero in the ideal case) for the correct interface and higher for other interfaces. Hence the interface location of the delamination can be determined, along with the axial location and size, by comparing the minimum values of the standard deviations for the different interfaces and selecting the one that has the lowest value. Table 4 lists the minimum standard deviations and the corresponding x-location and size values of the example shown in Figure 10. As can be seen, the standard deviation is the least minimum for interface 4, and increases as the interface considered moves further away from the actual one. There is a possibility that certain planes representing the measured frequency shifts may not intersect the 3D plots or those intersection curves do not meet at all, for instance interface 1 here, so there is no meeting point of the intersection curves and these are indicated by 'nan' in the table. It is worth noting that, even for the incorrect interfaces, the predicted locations are quite close to the actual delamination location, while the predicted size increases from the mid-plane to the outermost interface.

6. Validation of the graphical method

6.1. Numerical validation

To validate the proposed graphical method to estimate delamination parameters, seven test cases were generated using the FE model described in section 2 for a quasi-isotropic $[0/-45/45/90]_s$ CFRP simply supported beam with delamination parameters that matched those of the test samples with artificial delaminations employed in the experiments (Table 1). The database generated from FE model covered a range of 0.14:0.02:0.5 for x/L and 0.06:0.02:0.28 for a/L for each of the four interfaces. Note that due to symmetry in the simply supported condition, we need to generate data only for half the length of the beam; the data for delamination size was restricted to 28% of the length as the maximum size expected was under 25%. The first seven bending frequencies obtained from the FE model are used as inputs in the graphical method of inverse solution to predict the delamination parameters. The actual and predicted values of interface, x location and size are listed in Table 5 along with the percentage errors in the predictions of the x-location and

Table 4. Locations and standard deviations of intersection plots for interfaces 1 to 4 in example beam.

	Interface 1	Interface 2	Interface 3	Interface 4	Actual	Prediction
Std[a]	Nan[b]	0.802	0.241	0.027	Interface 4	Interface 4
X-location (%)	Nan	40.08	39.96	39.99	40	39.99
Size (%)	Nan	20.74	16.67	15.98	16	15.98

[a]Standard deviation, [b]nan indicates there is no intersection point.

Table 5. Comparison of actual and predicted delamination parameters in simply supported beams using numerical validation data.

	Actual			Predicted			Error %	
Beam ID	Interface	x/L (%)	a/L (%)	Interface	x/L (%)	a/L (%)	x/L	a/L
1#	4	21.53	11.57	4	21.51	11.56	0.02	0.01
2#	3	21.68	12.79	3	21.67	12.38	0.01	0.12
3#	2	20.85	13.62	2	20.84	13.61	0.01	0.01
4#	2	46.4	24.86	2	46.4	24.87	0	−0.01
5#	2	45.64	18.32	2	45.63	18.32	0.01	0
6#	2	46.06	12.65	2	46.06	12.66	0	−0.01
7#	1	20.75	14.24	1	20.73	14.23	0.02	0.01

Table 6. Standard deviations at each interface and corresponding x-location and size (simply supported experimental beams).

	Interface 1			Interface 2			Interface 3			Interface 4		
Beam ID	Std	*x*/*L* (%)	*a*/*L* (%)	Std	*x*/*L* (%)	*a*/*L* (%)	Std	*x*/*L* (%)	*a*/*L* (%)	Std	*x*/*L* (%)	*a*/*L* (%)
1#	Nan	Nan	Nan	**1.19**	19.8	16.9	1.45	20.2	14.2	1.43	20.4	13.5
2#	Nan	Nan	Nan	1.14	22.7	16.9	**0.94**	22.9	14.0	0.96	22.9	13.3
3#	0.94	21.0	21.3	**0.37**	20.1	14.7	0.53	20.7	12.0	0.58	20.8	11.4
4#	Nan	Nan	Nan	**1.32**	45.7	26.3	1.95	45.0	21.8	1.52	45.0	20.4
5#	Nan	Nan	Nan	**0.32**	46.7	18.1	0.84	46.5	15.2	0.80	46.5	14.5
6#	1.01	49.0	20.7	0.31	45.7	14.6	0.25	46.3	11.7	**0.15**	46.4	11.2
7#	0.38	48.0	15.2	0.49	47.3	10.8	**0.29**	47.7	9.11	0.46	47.6	8.46

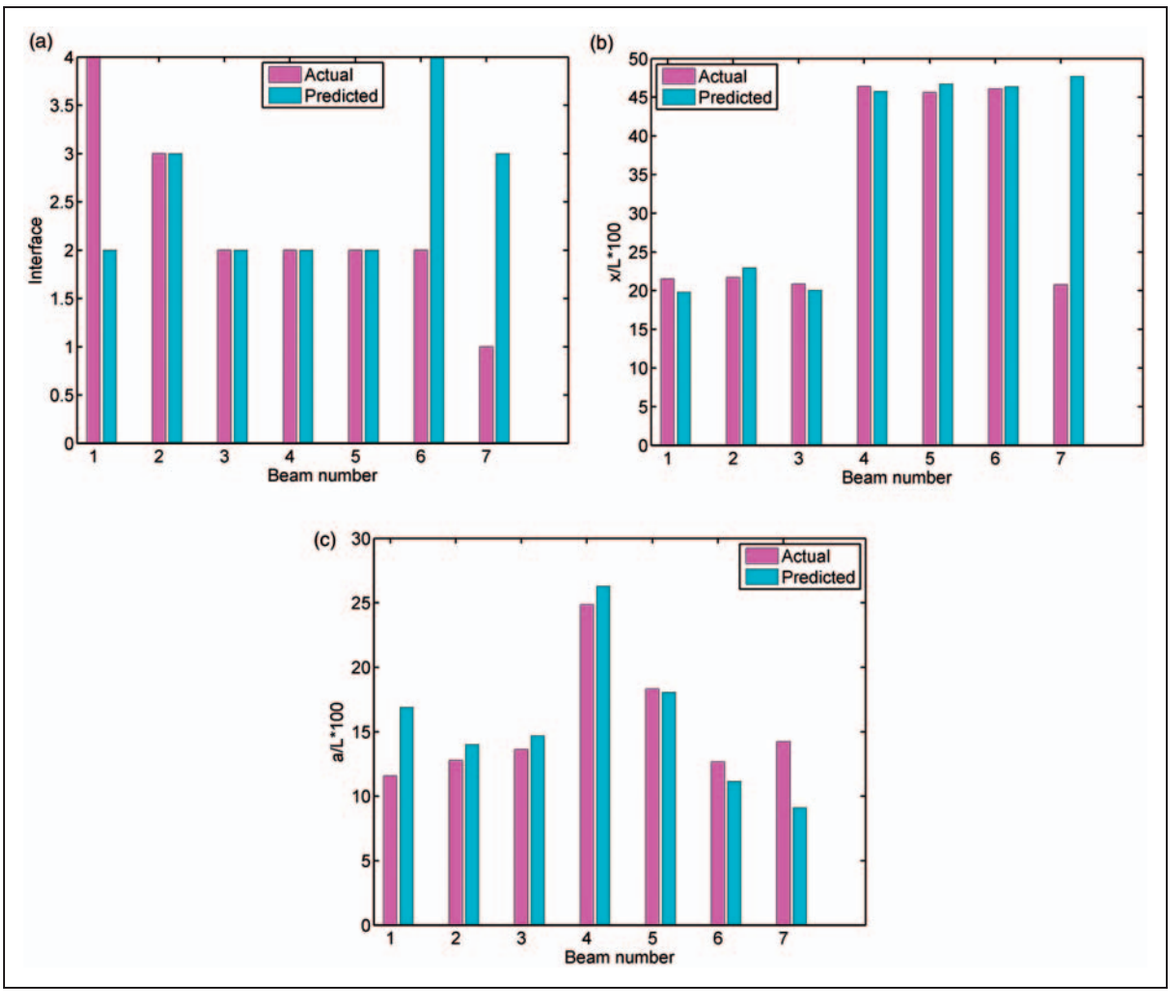

Figure 11. Comparison of actual delamination parameters with those predicted from measured frequency shifts for simply supported beams (a) interface, (b) x-location and (c) size.

Table 7. Comparison of actual and predicted delamination parameters for cantilever beams.

	Actual			Predicted			Error %	
Beam ID	Interface	*x*/*L* (%)	*a*/*L* (%)	Interface	*x*/*L* (%)	*a*/*L* (%)	*x*/*L*	*a*/*L*
1#	4	18.41	11.49	4	18.0	11.21	0.41	0.28
2#	3	18.56	12.7	4	19.0	9.4	−0.44	3.3
3#	2	17.74	13.52	3	18.93	10.45	−1.2	3.1
4#	2	43.1	24.68	2	14.57	22.46	28.5	2.2
5#	2	42.35	18.19	3	41.43	16.74	0.92	1.5
6#	2	42.77	12.56	4	42.93	11.41	−0.16	1.2
7#	1	17.65	14.14	4	14.73	8.2	2.9	5.9

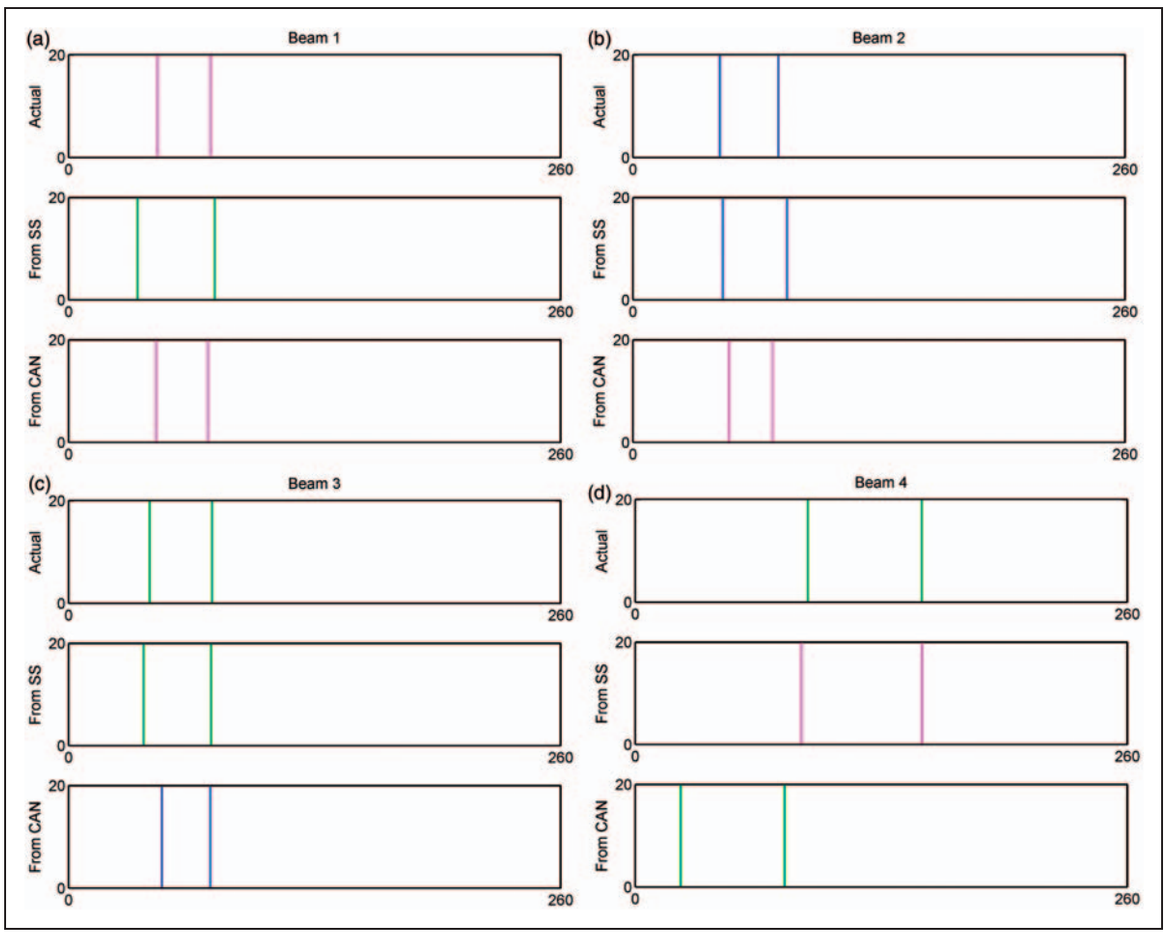

Figure 12. Schematic of actual delamination and those predicted from simply supported and cantilever beams.

delamination size. As can be seen, with the numerically simulated test data, the interface is predicted with 100% accuracy, while errors in the delamination size and x-location are very small (generally less than 0.15%). Please note that the errors here are the discrepancies between actual and predicted parameters which are already normalised with respect to the length of beam (this avoids the dependency of the

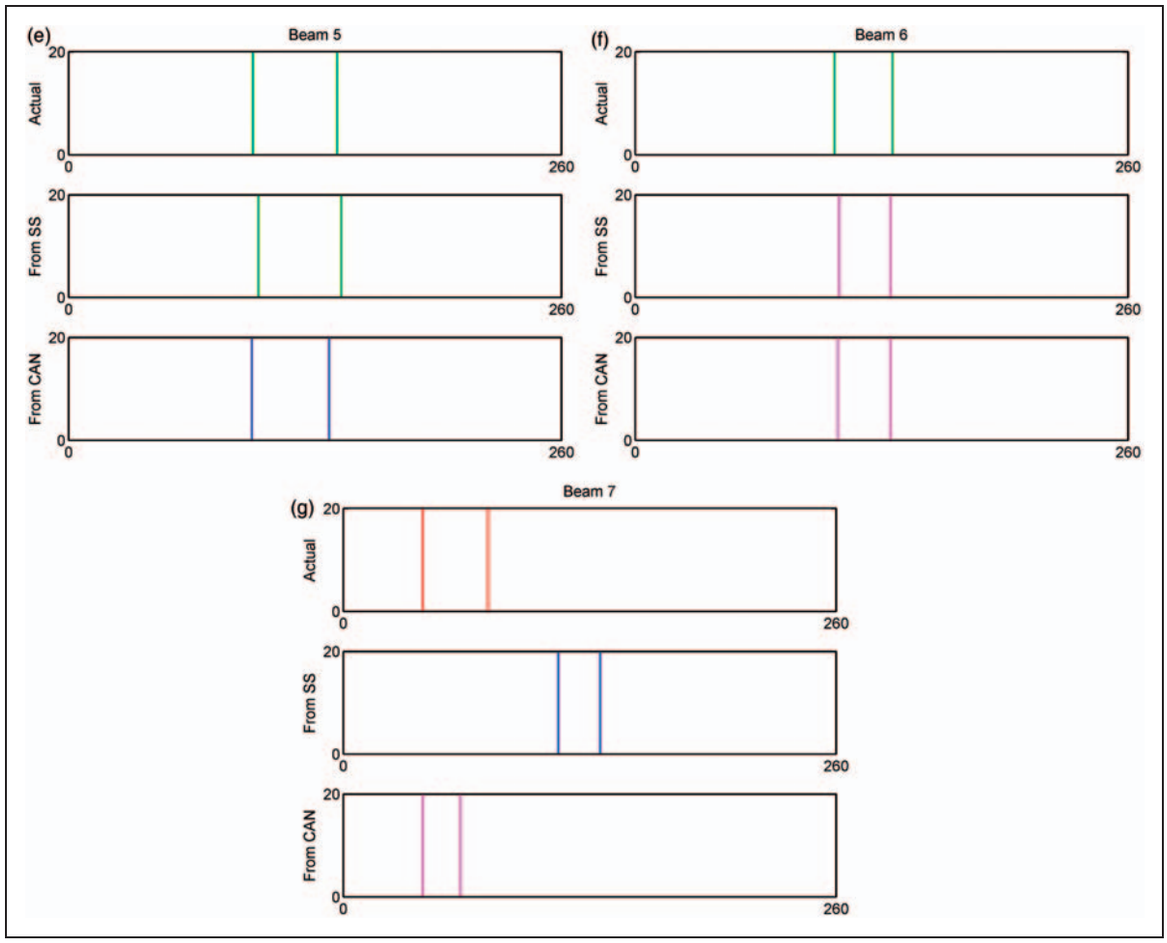

Figure 12. Continued.

error estimated on the origin of the x coordinate). The predictions of delamination parameters for the cantilever beams are also equally good when numerically predicted frequency shifts are employed in validation test cases.

6.2. Experimental validation

6.2.1. Simply supported beams. Following the methodology in Section 5.2, the three delamination parameters, size, x-location and interface are predicted using the measured frequencies of delaminated simply supported beams (Table 2). Table 6 lists the minimum standard deviations between the intersection curves at the planes of measured frequencies for each interface for each delaminated simply supported beam tested and the corresponding values of x-location and delamination size. The interface location is predicted based on the least minimum standard deviation which is highlighted in bold in Table 6 for each specimen. The comparison between the predicted and actual delamination parameters is shown graphically using bar charts in Figure 11(a)–(c) for interface, x-location and size respectively. As can be seen from Figure 11(a), only in four out of seven cases the interface locations are predicted correctly. The predicted values of x-location and size are quite close to the actual values with errors of less than 2% in most cases, except for the x-location of beam 7 (27% errors) and size of beam 1 and beam 7 (5.3% and 5.1% respectively). However, if the correct interface location is known and the corresponding values of x-location and size chosen from Table 6 for that interface, the prediction errors in size and location in these cases will be lower.

6.2.2. Cantilever beams. The delamination parameters estimated using the graphical technique from measured frequency shifts for the cantilever beams tested are listed in Table 7, along with their actual values and percentage errors in x-location and size prediction. The interface predictions are correct only for

beams 1 and 4. The discrepancies between the predicted and actual x-locations, however, are within 2%, except for beam 4 (over 28% error) and beam 7 (3% error). The errors in prediction of delamination size are within 5% in all cases except for beam 7 for which the error is 6%.

In order to facilitate comparison of the delamination parameters estimated using the graphical technique from frequency measurements under the different boundary conditions (S.S. and cantilever), the actual and predicted delaminations are shown to scale schematically for the beams tested in Figure 12. The interfaces are indicated using the colour codes: red - interface 1; green - interface 2; blue - interface 3 and magenta - interface 4. For each beam, the actual delamination is shown at the top; with the prediction for the simply supported boundary condition in the middle and the estimation for the cantilever boundary condition at the bottom. As can be seen, the interface prediction is incorrect (different colours) in more than half the cases suggesting that present method is not reliable for interface prediction in real beams. However, the location and size of the delamination have been estimated with good accuracy in most cases, except for beams 4 and 7 where large discrepancies either in location or size are found. This may be because beam 4 has the largest delamination and the delamination in beam 7 is in interface 1 which is closest to the surface. According to Luo and Hanagud (2000) and Lu et al. (2001) when the delamination is large and close to the beam surface, separation between the sub-laminates can occur during vibration and nonlinear effects must be taken into consideration, which is not done in the current FE model.

7. Conclusions

This paper presents a frequency based vibration monitoring system for laminated composites using a graphical approach to solve the inverse problem of estimating delamination interface, length-wise location and size. The graphical technique is computationally inexpensive and quick, since it solves the inverse problem without iterations or network training, unlike the use of optimisation or neural network. For generating the database to solve the inverse problem, finite element model of delaminated beams was built with added contact elements to prevent penetration and separation of the sub-laminates. From 3D plots of frequency change function, it is found that, depending on the given size of delamination is small or large the frequency shift may have opposite trend versus span-wise location. This reveals that delamination effect on frequencies can be stronger in the regions with high curvature or high shear subject to the delamination size. Validation of the graphical technique with numerically simulated data showed that the method can identify all three parameters accurately. However, the experimental validations of the delamination detection technique, with measurements on simply supported and cantilever beams, show that, in practice, the delamination interface is hard to predict correctly, but the x-location and size can be predicted mostly with errors of less than 5% even when the interface has not been correctly predicted.

It may be noted that in the experimental validation, the frequency shifts are calculated using frequencies measured on delaminated beams and frequencies for the undamaged beam computed from FE simulation. This suggests that the present method for delamination assessment does not require prior knowledge of the frequencies of the undamaged structure, provided it can be modelled with reasonable accuracy. It is also possible to detect and assess multiple delaminations by taking a previous set of measurements as baseline, provided that delaminations don't occur simultaneously. As the graphical technique is newly introduced for detection of delaminations in composites, its robustness needs to be studied before it can be applied as SHM in real life with confidence. A sensitivity analysis, using the addition of artificial random noise to simulate the measurement errors in measured frequencies is being conducted and will be reported in a future work along with comparison to other inverse algorithms.

Acknowledgment

Zhifang Zhang thanks the UNSW Canberra and CSC for sponsorship for her PhD study in Australia.

Funding

This research received tuition remission scholarship from UNSW Canberra and living expenses from China Scholarship Council (CSC).

References

Adams RD and Cawley P (1978) A vibration technique for non-destructively assessing the integrity of structures. *Journal Mechanical Engineering Science* 20: 93–100.

Advanced Composite Group Materials Database-MTM57/Panex35 (2004) ACG Technical Center. Heanor, Derby, UK.

Altenbach H, Altenbach J and Kissing W (2004) *Mechanics of Composite Structural Elements*. New York: Springer.

Chakraborty D (2005) Artificial neural network based delamination prediction in laminated composites. *Materials & Design* 26: 1–7.

Della CN and Shu D (2007) Vibration of delaminated composite laminates: A review. *Transactions of the ASME* 60.

Doebling SW and Farrar CR (1996) Damage Identification and Health Monitoring of Structural and Mechanical Systems from Changes in their Vibration Characteristics:

A Literature Review. Los Alamos National Laboratory Report.

Fan W and Qiao P (2010) Vibration-based damage identification methods: A review and comparative study. *Structural Health Monitoring* 10: 83–111.

Fritzen CP (2005) Vibration-based structural health monitoring-concepts and applications. *Key Engineering Materials* 293–294: 3–20.

Grouve WJB, Warnet L, Boer Ad, et al. (2008) Delamination detection with fibre Bragg gratings based on dynamic behaviour. *Composites Science and Technology* 68: 2418–2424.

Ihesiulor OK, Shankar K, Zhang Z, et al. (2012) Validation of algorithms for delamination detection in composite structures using experimental data. *Journal of Composite Materials* 48(8): 969–983.

Islam AS and Craig KC (1994) Damage detection in composite materials using piezoelectric materials. *Smart Materials and Structures* 3: 318–328.

Kessler SS, Spearing SM and Atalla MJ (2002) Damage detection in composite materials using frequency response methods. *Composites Part B: Engineering* 33: 87–95.

Kim JT and Stubbs N (2003) Crack detection in beam-type structures using frequency data. *Journal of Sound and Vibration* 259: 145–160.

Lu X, Lestari W and Hanagud S (2001) Nonlinear vibrations of a delaminated beam. *Journal of Vibration and Control* 7: 803–831.

Luo H and Hanagud S (2000) Dynamics of delaminated beams. *International Journal of Solids and Structures* 37: 1501–1519.

Montalvao D, Maia NMM and Ribeiro AMR (2006) A review of vibration-based structural health monitoring with special emphasis on composite materials. *The Shock and Vibration Digest* 38: 295–324.

Montalvao D, Ribeiro AMR and Duarte-Silva J (2009) A method for the location of damage in a CFRP plate using damping. *Mechanical Systems and Signal Processing* 23: 1846–1854.

Mottershead JE and Friswell MI (1993) Model updating in structural dynamics: A survey. *Journal of Sound and Vibration* 167: 347–375.

Mujumdar P and Suryanarayan S (1988) Flexural vibrations of beams with delamination. *Journal of Sound and Vibration* 125: 441–461.

Okafor AC, Chandrashekhara K and Jiang YP (1996) Delamination prediction in composite beams with built-in piezoelectric devices using modal analysis and neural network. *Smart Materials and Structures* 5: 338–347.

Owolabi GM, Swamidas ASJ and Seshadri R (2003) Crack detection in beams using changes in frequencies and amplitudes of frequency response functions. *Journal of sound and vibration* 265: 1–22.

Patil DP and Maiti SK (2005) Experimental verification of a method of detection of multiple cracks in beams based on frequency measurements. *Journal of Sound and Vibration* 281: 439–451.

Raghavan A and Cesnik CES (2007) Review of guided-wave structural health monitoring. *The Shock and Vibration Digest* 39: 91–114.

Ramkumar RL, Kulkarni SV and Pipes RB (1979) Free vibration frequencies of a delaminated beam. *Reinforcing the future*.

Salawu OS (1997) Detection of structural damage through changes in frequency: A review. *Engineering Structures* 19: 718–723.

Sohn H, Farrar CR and Hemez FM (2003) A review of Structural Health Monitoring Literature: 1996–2001. *Los Alamos National Laboratory Report*. 1–307.

Springer WT, Lawrence KL and Lawley TJ (1988) Damage assessment based on the structural frequency-response function. *Experimental Mechanics* 28: 34–37.

Su Z, Ling H, Zhou L, et al. (2005) Efficiency of genetic algorithms and artificial neural networks for evaluating delamination in composite structures using fibre Bragg grating sensors. *Smart Materials and Structures* 14: 1541–1553.

Swanson J (2009) Modal analysis. In: *ANSYS User's Manual*.

Tracy JJ and Pardoen GC (1988) Effect of delamination on the natural frequencies of composite laminates. *Journal of Composite Materials* 23: 1200–1216.

Valoor MT and Chandrashekhara K (2000) A thick composite-beam model for delamination prediction by the use of neural networks. *Composites Science and Technology* 60: 1773–1779.

Wang J and Liu Y (1982) Vibration of split beams. *Journal of sound and vibration* 84: 491–502.

Wei Z, Yam LH and Cheng L (2005) Delamination asessment of multilayer composite plates using model-based neural networks. *Journal of Vibration and Control* 11: 607–625.

Xiang J and Liang M (2012) A two-step approach to multi-damage detection for plate structures. *Engineering Fracture Mechanics* 91: 73–86.

Xiang J, Matsumoto T, Wang Y, et al. (2013) Detection damages in conical shells using curvature mode shape and wavelet finite element method. *International Journal of Mechanical Sciences* 66: 83–93.

Yan YJ, Cheng L, Wu ZY, et al. (2007) Development in vibration-based structural damage detection technique. *Mechanical Systems and Signal Processing* 21: 2198–2211.

Yang Z, Chen X, Yu J, et al. (2013) A damage identification approach for plate structures based on frequency measurements. *Nondestructive Testing and Evaluation* 28: 321–341.

Zhang Z, Shankar K, Tahtali M, et al. (2010) Vibration modelling of composite laminates with delamination damage. In: Burgess M and Davey J (eds) *20th International Congress on Acoustics, ICA 2010*. Sydney, Australia.

Zhang Z, Shankar K, Tahtali M, et al. (2011) Vibration monitoring of composite laminates with delamination damage. *18th International Conference on Composite Materials, ICCM18*. Jeju Island, Korea.

Zou Y and Tong L (2000) Vibration-based model-dependent damage(delamination) identification and health monitoring for composite structures - A review. *Journal of Sound and Vibration* 230: 357–378.